frontiers | Frontiers in Mechanical Engineering

TYPE Original Research
PUBLISHED 03 February 2026
DOI 10.3389/fmech.2025.1727981

OPEN ACCESS

EDITED BY
J. P. Panda,
University of Notre Dame, United States

REVIEWED BY
Andaç Batur Çolak,
Niğde Ömer Halisdemir University, Türkiye
Ahmed Refaie Ali,
University of Menoufia, Egypt

*CORRESPONDENCE
Varesa Chuwattanakul,
varesa.ch@kmitl.ac.th

RECEIVED 19 October 2025
REVISED 20 December 2025
ACCEPTED 22 December 2025
PUBLISHED 03 February 2026

CITATION
Kumar Pant P, Chamoli S, Pant N, Joshi H, Rana S, Kumar Pathak M, Chuwattanakul V and Eiamsa-ard S (2026) Analysis of fluid flow across a 2D bluff body in a tandem arrangement with varying aspect ratios near a moving wall. *Front. Mech. Eng.* 11:1727981. doi: 10.3389/fmech.2025.1727981

Analysis of fluid flow across a 2D bluff body in a tandem arrangement with varying aspect ratios near a moving wall

Pawan Kumar Pant[1], Sunil Chamoli[1], Naval Pant[1], Hitesh Joshi[1], Saurav Rana[1], Manoj Kumar Pathak[1], Varesa Chuwattanakul[2]* and Smith Eiamsa-ard[3]

[1]Department of Mechanical Engineering, Govind Ballabh Pant Institute of Engineering and Technology, Pauri, India, [2]School of Engineering, King Mongkut's Institute of Technology Ladkrabang, Bangkok, Thailand, [3]School of Engineering and Industrial Technology, Mahanakorn University of Technology, Bangkok, Thailand

This study numerically investigates the flow characteristics around single and tandem cylinders positioned in close proximity to a moving wall at a Reynolds number of *Re* = 100. Using the finite volume method, simulations were performed for aspect ratios (AR) ranging from 1 to 5, while maintaining a fixed gap ratio (G/A = 0.5) and spacing ratio (S/A = 0.5). The results demonstrate that the moving wall significantly influences flow dynamics and stabilizes the wake. For an aspect ratio of 1, the merging of shear layers leads to the formation of elongated, steady vortices. As the aspect ratio increases from 2 to 5, the wake becomes increasingly smooth and the magnitude of positive vortices decreases, resulting in steady wake formation without significant oscillations. Force analysis reveals that the upstream cylinder exhibits chaotic drag (C_d) and lift (C_L) coefficients, whereas the downstream cylinder shows a consistent trend. Notably, the upstream cylinder maintains a higher drag coefficient than the downstream cylinder, with both being lower than that of a single isolated cylinder. The observed suppression of vortex shedding is primarily attributed to the interaction and coupling of shear layers between the moving wall and the cylinders, identifying shear alignment rather than viscous damping as the core mechanism of wake control.

KEYWORDS

tandem cylinders, moving wall, vortex suppression, shear layer interaction, wake dynamics

1 Introduction

Extensive research has been conducted on flow around bluff bodies near moving boundaries, a topic of both fundamental interest and considerable importance in engineering applications. When fluid flows over a bluff body, vortices or swirling patterns are generated on both sides, and the structure of these vortices evolves with changing Reynolds numbers. Key parameters, such as the size, orientation, shape, and the gap between cylinders (interspatial distance), play a critical role in shaping the vortex structures that emerge. The study of vortex shedding near bluff bodies has significant real-world applications, including chimneys, transmission towers, suspension bridges, high-rise buildings, marine pilings, submarine periscopes, and underwater structures.

Vortices in the wake of these bodies produce fluctuating pressures that cause the structures to vibrate or oscillate, a phenomenon known as vortex-induced vibration (VIV). VIV is a significant issue, as it can lead to fatigue, structural damage, or even catastrophic failure. Current research has expanded beyond stationary walls to examine how moving boundaries near bluff bodies affect vortex shedding. When a moving boundary is present, it can significantly alter the frequency and amplitude of vortex shedding, leading to increased vibrations and a heightened risk of structural failure. Understanding these interactions is crucial for enhancing the design and performance of structures subjected to fluid flow. Rajpoot et al. (2021) examined the influence of a moving wall on vortex shedding for tandem square cylinders. They reported that varying spacing and gap ratios significantly affect vortex shedding behavior. The drag coefficients are highest for single cylinders, followed by cylinders located upstream and downstream. Dhinakaran (2011) found that as the gap ratio decreases, vortex shedding stabilizes and heat transfer improves for square cylinders near moving walls. Bhattacharyya and Maiti (2005) observed that in the case of square cylinders near a moving boundary, vortex shedding suppression does not occur, unlike with stationary boundaries, even at low gap ratios.

This behavior is particularly relevant in real-world scenarios, where tandem configurations are common. Barry et al. (2016) indicated that such setups are encountered in intelligent transport systems and seabed pipelines. Flow past tandem circular cylinders has been studied by Yang and Stremler (2019), who investigated configurations and cross-sectional geometries, demonstrating that these parameters strongly influence wake dynamics. Similarly, Sarkar et al. (2021) analyzed unsteady flow across semi-circular and circular cylinders, showing that incidence angles and Reynolds numbers play a critical role in altering the wake structures. In another investigation, Chen et al. (2020) used the immersed boundary method to simulate vortex-induced vibrations between two circular cylinders near a stationary wall, revealing that proximity affects both vortex shedding frequency and amplitude. Zhao (2021) extended this by studying flow between a circular cylinder and a downstream sphere, focusing on the impact of varying gap ratios on vortex shedding and fluid forces.

Further experimental and numerical research highlights the importance of geometric variations and external flow conditions. Bearman and Zdravkovich (1978)experimentally investigated flow around a circular cylinder near a plane boundary, finding that vortex shedding is suppressed when the gap ratio is small, but it remains stable with larger gaps. Huang and Sung (2007) numerically simulated flow near a moving wall, identifying critical transitions in lift and drag forces based on gap ratios. This finding is consistent with the observations of Cheng et al. (2007), who used the lattice Boltzmann method to simulate shear flow over square cylinders, demonstrating that the vortex shedding frequency depends heavily on Re and shear rate. Likewise, Cheng et al. (2005) and Sen et al. (2011) reported that for very low Reynolds numbers, flow remains laminar and two-dimensional without separation. Kalita and Ray (2009) developed a compact numerical method for solving the 2D Navier-Stokes equations on polar grids to model thick fluid flows around circular cylinders. Lankadasu and Vengadesan (2008) observed that for square cylinders, unsteady, three-dimensional flow starts at Re = 47, while Saha (2013) found that vortex shedding becomes three-dimensional at Re > 161, leading to increased drag and lift fluctuations. The two-dimensional model is used to perform the simulations at a Reynolds number Re = 100. As it was previously demonstrated, in bluff-body flows with Re ≤ 100, the wake is still essentially two-dimensional, and all the instabilities in the wake with three dimensions are only observed at further Reynolds numbers (Rajpoot et al., 2021). Thus, it is reasonable to use a two-dimensional formulation to describe the necessary dynamics of wakes at this Reynolds number. Even though the moving wall creates a significant near-wall shear, the flow regime in the present case does not reach the level at which spanwise instabilities can become important, as documented in the literature.

In terms of vortex suppression and control methods, Saha and Shrivastava (2015) demonstrated that blowing jets past a square cylinder reduced vortex shedding, with parabolic velocity profiles being more effective than uniform profiles. Wu and Choi (2021) explored the effects of steady and time-periodic blowing over a circular cylinder at Re = 21,000, achieving drag reductions of up to 68% by inducing vortex lock-on phenomena. Seo et al. (2023) employed large eddy simulations to investigate the effects of tab configurations on a circular cylinder, achieving a 14% reduction in mean drag and a 95% reduction in lift fluctuations. Zhu et al. (2023) analyzed the flow past a circular cylinder with bilateral splitter plates at Re = 100, identifying five distinct vortex shedding regimes that depend on the gap ratio and inclination angle. They observed that the lift decreases significantly with an increased angle.

Investigations into the flow dynamics around cylinders of various shapes and orientations have also contributed to a broader understanding of vortex shedding. Lankadasu and Vengadesan (2011) explored the shift of wake flow from 2D to 3D in a square cylinder exposed to linear shear. Akansu and Fırat (2010) experimentally investigated flow around square prisms at high Reynolds numbers, finding that injection from the base reduces drag and alters wake dynamics. Zhang and Balachandar (2006) studied the effects of transverse spacing on the critical Reynolds number for two cylinders, showing that spacing significantly impacts wake structures and vortex shedding. Yen et al. (2008) examined the impact of spacing ratios, rotational angles, and Reynolds numbers on flow characteristics in water tanks with square cylinders. Rahman et al. (2007) investigated unsteady wakes behind a circular cylinder, providing insights into dynamic pressure and velocity fields.

In addition to these studies, Franke et al. (1990) performed numerical calculations of laminar vortex shedding at low Reynolds numbers, finding that flow remains laminar at Re < 1,000. Experimental work by Kiya et al. (1980) showed that for shear flows, the critical Reynolds number for vortex shedding is higher than for uniform flows, a finding confirmed by Cheng et al. (2007), who reported a strong dependence of vortex shedding on both Reynolds number and shear rate. Davis and Moore (1982). Numerically examined vortex shedding in rectangular bodies, finding that Strouhal numbers align well with experimental data

at lower Reynolds numbers. Sohankar (2008) explored vortex shedding in rectangular cylinders with varying side ratios and found that geometric changes significantly influence wake dynamics. Hwang and Sue (1998) simulated uniform shear flow around square cylinders, while Bearman (1984) and Sasmal and Chhabra (2011) provided early insights into swirling patterns in bluff bodies and heat transfer from square cylinders in power-law fluids.

Recent advances in numerical simulations have further expanded our understanding of these complex flow phenomena. Zhang et al. (2022) conducted 3D simulations of flow around three cylinders at super-critical Reynolds numbers, focusing on the sensitivity of vortex structures to spacing ratios. Zhu et al. (2019) used direct numerical simulations to study flow past slotted cylinders, showing that slot configurations can significantly affect vortex formation and wake behavior. Flow control has emerged as an important research focus on improving aerodynamic performance through the control of separation, circulation and wake interactions around bluff bodies. Pulsed jets serve as an effective active technique for regulating aerodynamic coefficients and eliminating vortex shedding, provided the appropriate excitation frequencies are applied (Abdolahipour, 2023). The cutting-edge ideas, such as the modulated pulsed jet actuation of multi-body lifting designs (Abdolahipour et al., 2022a; Abdolahipour et al., 2022b) and the full-scale implementation, such as the blown-jet control of the vertical tail of commercial planes (Taleghani et al., 2025), further demonstrate the increased interest and relevance of flow-control techniques. In this regard, the current research takes into consideration wall movement and geometric length change as a passive flow-controlling methodology that has the ability to affect the formation of wakes and force properties as an alternative to popular methods of jet-actuation (Abbasi et al., 2024). Recent aerodynamic studies focus on multi-objective optimization and machine learning of complex multi-body flows, making wall-motion control an attractive passive approach to wake control a promising area of research in the near future (Shams Taleghani and Torabi, 2025; Sha et al., 2025).

Despite the many investigations conducted on fluid flow over bluff body formations in tandem, most of these have been on stationary boundary configurations with the traditional no-slip condition. Several authors, including Rajpoot et al. (2021), Barry et al. (2016), Yang and Stremler (2019), Zhao (2021), and Akansu and Fırat (2010), have exhaustively studied wake interactions, drag reduction mechanisms, and vortex shedding patterns for tandem-cylinder arrangements subjected to these conventional boundary conditions. Nevertheless, there is a substantial gap in research on how such flow phenomena are affected by moving boundaries. Few studies focus on moving wall effects, and they studied isolated bodies rather than those in a tandem configuration. This restriction is particularly notable because many real-world engineering implementations meet this condition, where multiple bodies are in proximity to moving surfaces, such as conveyor systems, rotating machinery, and other moving technologies. The present study addresses this research gap through a systematic investigation into the combined effects of tandem configurations and moving wall conditions on the flow characteristics and aerodynamic performance of 2D bluff bodies with varying aspect ratios. This study characterizes the interaction between wake dynamics and wall-induced shearing, resolving flow physics that are inherently absent in standard stationary boundary simulations.

Although prior studies have elaborately reported on the interactions of wakes and shedding of vortices of tandem cylinders when close to stationary walls (Rajpoot et al., 2021; Barry et al., 2016; Yang and Stremler, 2019; Zhao, 2021; Akansu and Fırat, 2010), the effect of change in aspect ratio when a moving boundary is present has not been clearly established. This gap in knowledge is especially important since changing the aspect ratio provides a fundamental change to the pressure field and shear layer formation around bluff bodies, and these changes are further altered by the shear exerted by the wall when the wall is moving as well (Okajima, 1982; Norberg, 1993). Unlike immobile wall structures where the no-slip conditions govern, the motion of the walls introduces new shear layers, which interact with the wakes of the cylinders, which radically changes the process of generating the vortices. These interactions are enhanced or minimized by the aspect ratio in terms of relative blockage caused by cylinders and relative shear caused by walls, but there is no systematic investigation of the effect of aspect ratio in improving the countermeasures in tandem configurations.

The practical relevance of investigating aspect ratio effects under moving-wall conditions lies in its broad range of critical engineering applications. In ground vehicle aerodynamics, moving ground simulation occurs in underbody flow around vehicles with different chassis geometries, and the aspect ratio has a direct effect on the drag, downforce, and aerodynamic stability (Ahmed et al., 1984; Hucho, 2013). High-speed rail systems also entail train underbody elements with varying aspect ratios in contact with the track (moving relative to the train) that influence aerodynamic loads, and other acoustic signatures (Raghunathan et al., 2002). Submarine or autonomous underwater vehicle (AUV) appendages in the sea, like in the relative wall motion, component aspect ratios influence hydrodynamic performance (Anthony and Turnock, 2007). In conveyor belt systems, the flow of materials is governed by the aspect ratio to separate flows and drag pressure in objects of different geometries under motion as to surfaces of the belt systems (Schlichting et al., 2017). Furthermore, microfluidic devices equipped with tandem obstacles of different aspect ratios adjacent to channel walls require accurate control of flow to manipulate particles and enhance mixing (Squires and Quake, 2005). Recent studies on heat transfer from tubes in crossflow, spanning Prandtl numbers of 0.7–500 and Reynolds numbers up to 2×10^6, highlight the influence of flow regimes and fluid properties on single tubes and tube banks (Žkauskas, 1987).

Based on the above considerations, our hypothesis is that as the aspect ratio of tandem square cylinders is increased about a moving wall, the vortex shedding and fluctuation of the force caused by the shear layer interaction and altered blockage effect will progressively decrease. In particular, at critical aspect ratios (AR > 2), we believe the region of wall-generated shear and lengthwise wakes will change the flow to unsteady periodic shedding to quasi-steady or steady wakes production and lead to much lower oscillations in drag of the downstream cylinder. It is expected that this transition will be

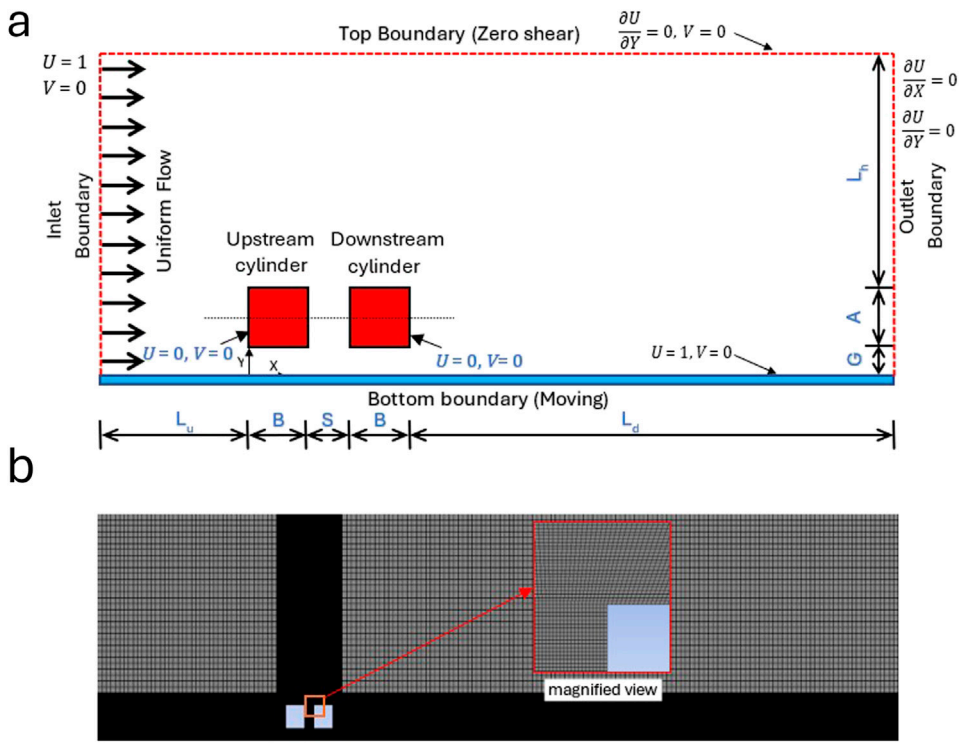

FIGURE 1
Representation of: **(a)** the computational domain used in this study, where A is the characteristic length and height of the cylinder, B is the cylinder width with B/A = AR, L_u is the upstream distance (10A), L_h is the top boundary distance (8A), and L_d is the downstream distance (40A); **(b)** mesh distribution.

achieved at lower spacing ratios compared to those reported in stationary wall cases, as the amplified shear layer merges with the aid of wall motion.

2 Flow configuration and objective of this study

Figure 1a shows a typical computational domain consisting of two infinitely long cylinders with a height of A and a width of B, arranged one behind the other in a tandem configuration near a moving plane wall. The velocity of the moving wall is similar to the free stream velocity, denoted by U_∞. When the velocity of the wall is less than the free-stream velocity the induced shear layer becomes weaker so that vortex suppression is delayed and higher aspect ratios are needed. On the other hand, increased wall velocity enhances near-wall shear and quicker merging of shear-layers resulting in vortex suppression at decreased aspect ratios. The vertical gap between the bottom surface of the cylinder and the moving wall is represented by G, whereas S denotes the spacing between the two cylinders. Uniform velocity profile of $U = 1$ and $V = 0$ is considered at the inlet.

A condition of zero shear $\frac{\partial U}{\partial y} = 0$, and V = 0 is provided at the top boundary. The bottom boundary is moving with the free stream velocity ($U = 1$ and $V = 0$), and the outlet boundary is treated as a pressure outlet. The cylinder's surface is treated as a no-slip wall. The distribution of the mesh within the computational domain is non-uniform, as shown in Figure 1b. The grid points are segmented into three distinct zones in both dimensions. A finer mesh is utilized to precisely capture the intricate flow characteristics close to the cylinders and the moving boundary, whereas a coarser mesh is employed in other regions. When AR = 1, the height A and width B are equal. When AR > 1, the width B expands as B = AR × A, while, maintaining a constant A and guaranteeing Re = 100 for all configurations. The Reynolds number remains constant as it is defined by the characteristic length A, while varying the aspect ratio (B/A) modifies the blockage ratio and the geometric confinement of the flow. The redistribution of width and height with an increase in the aspect ratio alters the locally imposed blockage on the flow and enhances near-wall interactions, particularly in the context of moving-wall conditions. An increase in the aspect ratios thus encourages good shear-layer coupling, longer recirculation zones and increased wake stabilization. The variations in vortex shedding and force coefficients are, therefore, attributable to the combined effects of geometric blockage and wall-generated shear, rather than changes in the Reynolds number.

Based on the detected research gap, the main aim of the proposed research is to systematically examine the effect of the aspect ratio (B/A = 1–5) on the unsteady laminar flow characteristics around tandem square cylinders placed close to a moving wall at Re = 100, with constant gap ratio (G/A = 0.5) and spacing ratio (S/A = 0.5). This investigation focuses on the impact

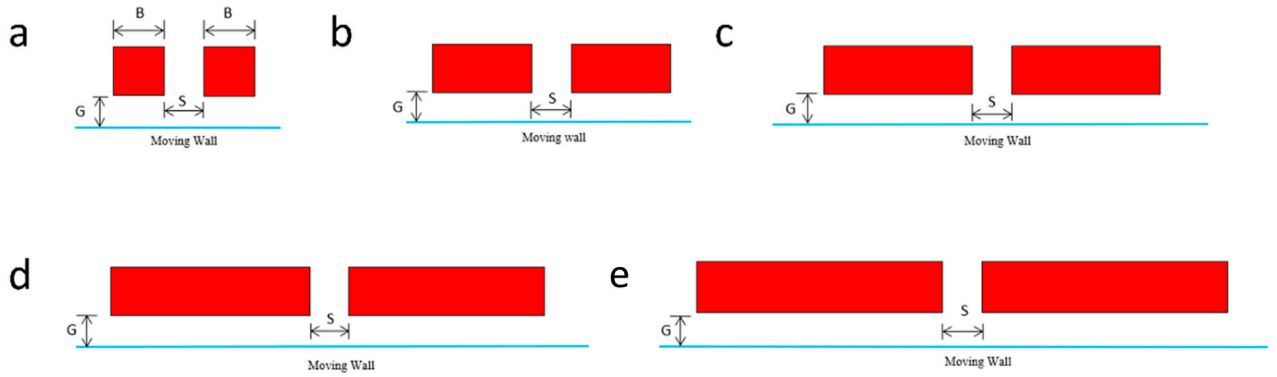

FIGURE 2
Cases in the present study: **(a)** Case 1: AR = 1; **(b)** Case 2: AR = 2; **(c)** Case 3: AR = 3; **(d)** Case 4: AR = 4; and **(e)** Case 5: AR = 5.

of aspect ratio modulation on vortex shedding control within moving wall configurations. Specifically, it examines aerodynamic force coefficients and their temporal behavior, the transition of wake structures into quasi-steady shedding, and the interaction between wall-generated shear layers and cylinder-generated vorticity. G/A = 0.5 and S/A = 0.5 are critical values of the ratio such that strong interference can occur, similar to ground clearances in automotive aerodynamics (usually 0.4–0.6 vehicle heights) (Ahmed et al., 1984). Reynolds number 100 is able to maintain the laminar and two-dimensional flow and capture the vortex dynamics vital in low-speed applications and microfluidic setups. Our hypothesis is that monotonic suppression of the intensity of vortex shedding will occur with aspect ratio increase, where a critical transition to quasi-steady wake formation will occur at AR 2-3 and above. Figure 2 shows the cases considered in the present study in terms of different aspect ratios, starting with 1.

3 Mathematical formulation

The equations that describe the two-dimensional unsteady, incompressible, constant viscosity flow across a tandem-cylinder system, namely, the continuity and momentum equations (in a non-dimensional form), are given as follows.

Continuity equation:

$$\frac{\partial U}{\partial X}+\frac{\partial V}{\partial Y}=0 \tag{1}$$

Momentum equations:

$$\frac{\partial U}{\partial \tau}+U\frac{\partial U}{\partial X}+V\frac{\partial U}{\partial Y}=-\frac{\partial P}{\partial X}+\frac{1}{Re}\left(\frac{\partial^2 U}{\partial X^2}+\frac{\partial^2 U}{\partial Y^2}\right),\text{and} \tag{2}$$

$$\frac{\partial V}{\partial \tau}+U\frac{\partial V}{\partial X}+V\frac{\partial V}{\partial Y}=-\frac{\partial P}{\partial Y}+\frac{1}{Re}\left(\frac{\partial^2 V}{\partial X^2}+\frac{\partial^2 V}{\partial Y^2}\right). \tag{3}$$

The above governing equations were non-dimensionalised using: $X=\frac{x}{A}$, $Y=\frac{y}{A}$, $\tau=\frac{tU_\infty}{A}$ $P=\frac{P}{\rho U_\infty^2}$, $U=\frac{u}{U_\infty}$, $V=\frac{v}{U_\infty}$

Reynolds (Re) is defined as:

$$Re=UA/\vartheta \tag{4}$$

The lift and drag coefficients are calculated as:

$$C_d=\frac{F_D}{0.5\rho U^2 A}, C_L=\frac{F_L}{0.5\rho U^2 A} \tag{5}$$

where F_D and F_L are the forces acting on the cylinder in the transverse and streamwise directions, respectively.

The vortex shedding frequency, which is determined by the Strouhal number (St), is obtained by applying the Fast Fourier transform (FFT) to the lift coefficient (C_L) time history.

$$St=\frac{fA}{U} \tag{6}$$

Two-dimensional flow's vorticity is computed as follows:

$$\omega_z=\nabla\times u=\frac{\partial v}{\partial x}-\frac{\partial u}{\partial y} \tag{7}$$

The time average and RMS value for any parameter between time points t_1 and t_2 can be found using the following formulas.

$$\varnothing_{avg}=\frac{1}{t_2-t_1}\int_{t_1}^{t_2}\varnothing dt \tag{8}$$

$$\varnothing_{RMS}=\sqrt{\int_{t_1}^{t_2}\left(\varnothing_i-\varnothing_{avg}\right)^2} \tag{9}$$

The average that was determined after ten full cycles.

4 Numerical details

A numerical simulation of uniform isothermal airflow over a tandem cylinder system near a moving wall was performed using the commercial CFD solver ANSYS FLUENT. This software utilizes the control volume method to solve the governing partial differential equations. A pressure-based, two-dimensional, time-dependent, viscous, laminar flow model with double precision is chosen to simulate the flow at a Reynolds number of 100. The Semi-Implicit Method for Pressure-Linked Equations (SIMPLE) scheme is used to couple the pressure and velocity fields. A second-order implicit

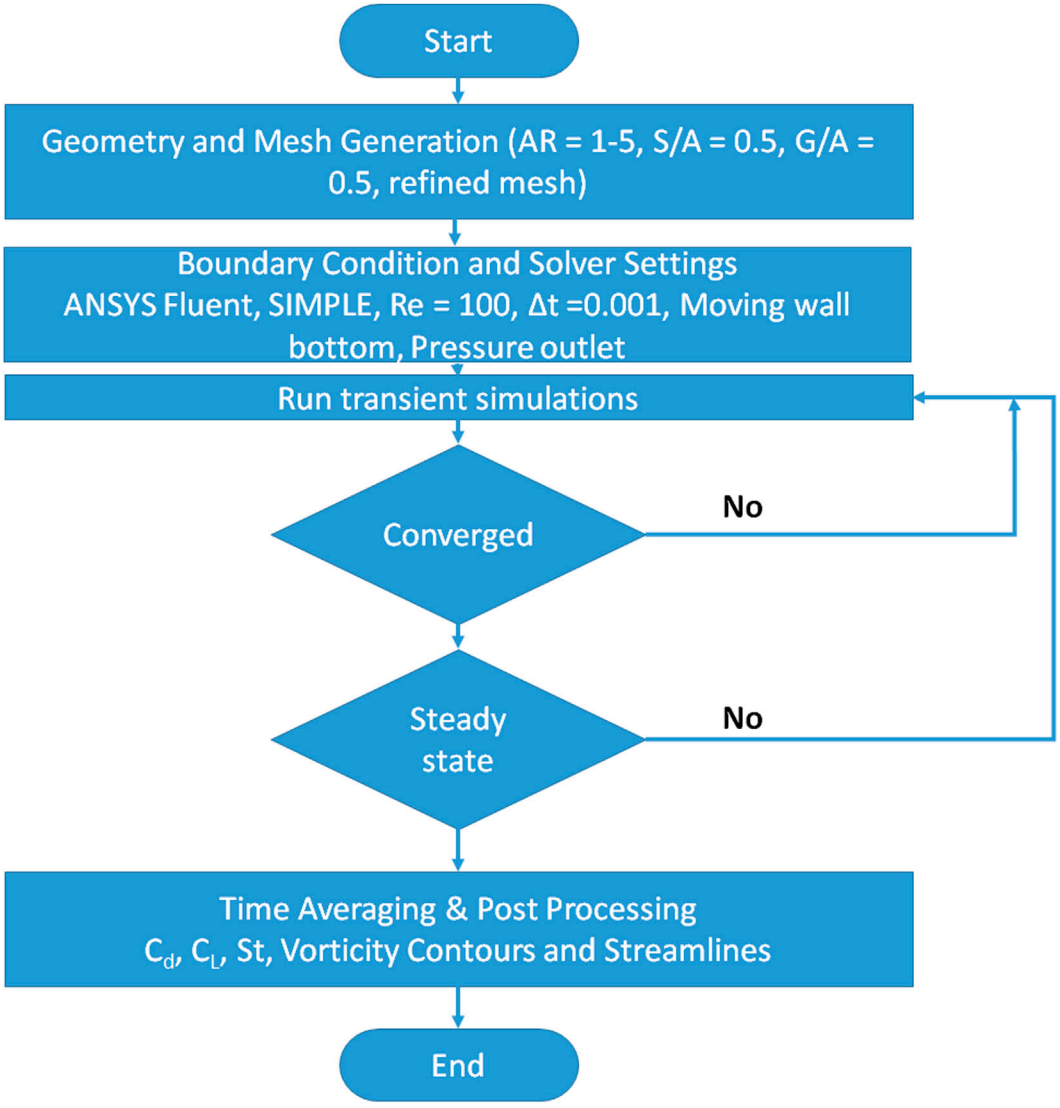

FIGURE 3
An illustration of the CFD methodology employed in this investigation.

method is used for the transient formulation, and a second-order upwind scheme is used for convective and transport terms. The time step is kept at 0.001 in all simulations, which meets the requirements of the Courant–Friedrichs–Lewy number (CFL). The simulations are considered converged when the residuals for the continuity and momentum equations fall below 10^{-6}. The dimensionless time step has also been clearly mentioned as $\frac{\Delta t U_\infty}{A} = 0.001$, where A is the height of cylinder and this will provide time accuracy in capturing the unsteady shedding of the vortex. A detailed flowchart demonstrating the CFD methods used in this investigation is shown in Figure 3.

TABLE 1 Mesh sensitivity and downstream boundary length (L_d) dependence test on drag (C_{d1} and C_{d2}) and lift (C_{L1} and C_{L2}) coefficients of tandem cylinders, and the Strouhal number (*St*) at a Reynolds number (*Re*) = 100 for an aspect ratio (AR) = 1 with fixed *S/A* and *G/A* ratio of 0.5.

L_d	*S/A* and *G/A* = 0.5				
	C_{d1}	C_{d2}	C_{L1}	C_{L2}	St
30*A*	1.8124	0.2177	0.5634	0.3033	0.1133
40*A*	1.9214	0.2289	0.5861	0.3257	0.1188
50*A*	1.9212	0.2298	0.5859	0.3258	0.1237

4.1 Mesh independence study

The inlet boundary is kept at a distance (L_u) 10*A* from the upstream cylinder, and the top boundary is kept (L_h) 8*A* from the top surface of the cylinders to avoid obstruction and potential influence on computational outcomes, Figure 1a. The influence of the distance of an outlet boundary from the downstream cylinder (L_d) on the drag (C_{d1} and C_{d2}) and lift (C_{L1} and C_{L2}) coefficients of tandem cylinders, and also on the Strouhal number

TABLE 2 Study of grid independence for *AR* = 1 at *Re* = 100 with *S/A* = 0.5 and *G/A* = 0.5.

Mesh type	Total cells	$\Delta y_{min}/A$	C_{d1}	C_{d2}	C_{L1}	C_{L2}	St
Coarse	45,000	0.010	1.8856	0.2145	0.5723	0.3189	0.1165
Medium	85,000	0.005	1.9214	0.2289	0.5861	0.3257	0.1188
Fine	135,000	0.0025	1.9228	0.2293	0.5868	0.3261	0.1190

(*St*) is tested for three distinct values of L_d viz., 30*A*, 40*A* and 50*A* at a Reynolds number (*Re*) = 100 for an aspect ratio (AR) = 1 with fixed *S/A* and *G/A* ratios of 0.5. These results are tabulated in Table 1. Finally, to reduce computational costs, a downstream boundary length of 40*A* is chosen and used for all cases in the present study. In the study, it has added specific mesh data of the total number of cells (about 85,000 case of AR = 1), the minimum grid spacing would be close to the walls of the cylinder (Δy_{min} = 0.005A, and minimum spacing would be close to the moving wall (Δy_{wall} = 0.008A). The values known as y + at the surface of the cylinders are kept as small as possible (under 1) to provide a true resolution of the laminar boundary layer at *Re* = 100. Table 2 has been added, presenting the grid independence study results for three mesh densities (coarse: 45,000 cells, medium: 85,000 cells, and fine: 135,000 cells), along with the corresponding C_d, C_L, and *St* values, to demonstrate mesh convergence. Mesh independence is confirmed by the medium mesh, which has about 85,000 cells, exhibiting force coefficient variation of less than 0.2% when compared to the fine mesh.

Additionally, as indicated in Table 3, a domain independence study was conducted by varying the upstream distance (L_u), top boundary distance (L_h), and downstream distance (L_d). The findings show that domain-independent solutions with computational efficiency are offered by L_u = 10A, L_h = 8A, and L_d = 40A.

Four non-dimensional time steps $\Delta t \cdot U\infty/A$ = 0.004, 0.002, 0.001, and 0.0005 were used in a time-step convergence investigation to ensure the results are independent of the temporal resolution. A comparison was made between the corresponding mean drag (C_d), lift (C_L), and Strouhal number (St) values. Since the difference between $\Delta t \cdot U\infty/A$ = 0.001 and 0.0005 was less than 0.5% for all force coefficients and St, $\Delta t \cdot U\infty/A$ = 0.001 was chosen for all simulations in order to balance computing cost and accuracy. Time-averaged drag and lift coefficients are calculated once the flow has reached a statistically steady state, which usually happens after ten cycles of vortex shedding. To guarantee mean value convergence, time averaging is then carried out over a minimum of ten full shedding cycles. Averaging is carried out over a dimensionless time period of τ = 200 (equivalent to $\Delta t \cdot U\infty/A$ = 200) in cases where vortex shedding is suppressed (AR ≥ 2).

4.2 Numerical simulation methodology validation

To validate the code employed in this study, calculations were performed for parameters such as the drag coefficient (C_d) and Strouhal number (*St*) under uniform flow conditions around an isolated square cylinder. The range of Reynolds numbers considered for this validation was 50 ≤ *Re* ≤ 150. These results are shown in Figure 4a. The numerical results obtained from the current simulations for the drag coefficient (C_d) and Strouhal number (*St*) of the isolated cylinder case are compared with those from literature studies (Rajpoot et al., 2021; Dhinakaran, 2011; Franke et al., 1990; Robichaux et al., 1999; Sharma and Eswaran, 2004; Shimizu and Tanida, 1978; Sohankar et al., 1998). The results obtained in the present study show a remarkable agreement with those of Robichaux et al. (1999). Likewise, the current findings for the Strouhal number (*St*) in Figure 4b demonstrate a favorable concurrence with the outcomes reported by Robichaux et al. (1999). Then, code verification is done for the case of an isolated cylinder near a moving wall (both top and bottom boundaries are moving). As shown in Figures 4c,d compare the drag coefficient (Cd) and Strouhal number (St) for the square cylinder near a moving wall within the range of 0.2 ≤ G/A ≤ 4 at a Reynolds number of 100. These values are also compared with the corresponding data from the literature. It is observed that there is a significant agreement between the obtained results and the literature. The present study's results closely align with those reported by Rajpoot et al. (2021) and Dhinakaran (2011).

TABLE 3 Study of computational domain independence for AR = 1 at Re = 100 with S/A = 0.5 and G/A = 0.5.

L_u	L_h	L_d	C_{d1}	C_{d2}	C_{L1}	C_{L2}	St
8A	8A	40A	1.9187	0.2275	0.5845	0.3241	0.1186
10A	8A	40A	1.9214	0.2289	0.5861	0.3257	0.1188
12A	8A	40A	1.9219	0.2291	0.5864	0.3259	0.1189
10A	6A	40A	1.9198	0.2281	0.5852	0.3248	0.1187
10A	10A	40A	1.9216	0.2290	0.5862	0.3258	0.1188

5 Results and discussion

In this study, the flow of fluid through single and tandem cylinders with a height of A is examined with constant S/A and G/A (=0.5) ratios, at *Re* = 100. The analysis focuses on the influence of the moving wall on the vortex shedding behind the single and tandem cylinders, considering different aspect ratios: AR = 1, 2, 3, 4, and 5.

5.1 Vortex shedding cycle: instantaneous vorticity contours

Figures 5, 6 show the contours of instantaneous vorticity, resulting from a cylinder in the presence of a moving wall. Fixed

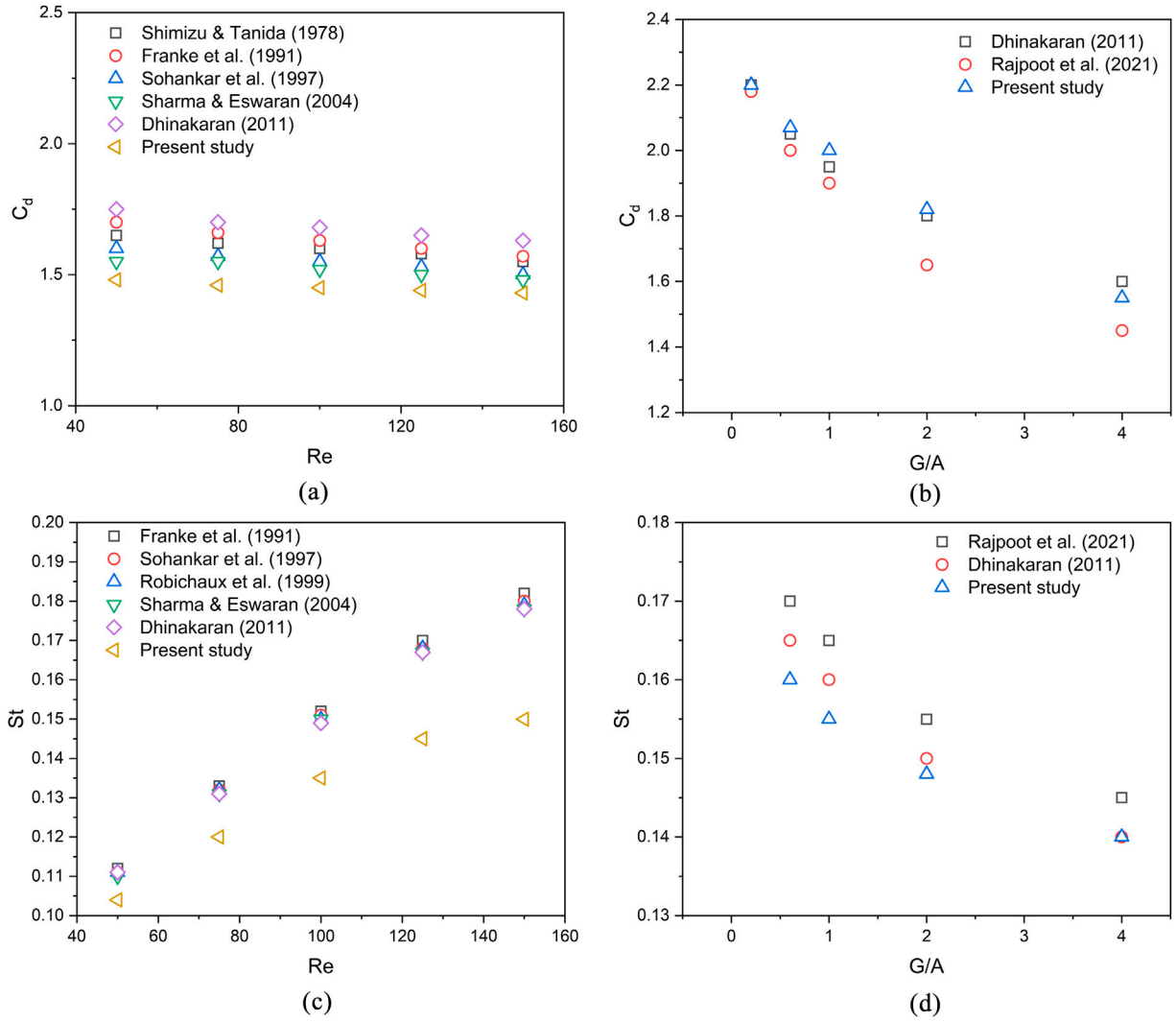

FIGURE 4
Comparison between the coefficient of drag (C_d), and Strouhal number (*St*) with the values reported in existing literature: **(a)** C_d for the fluid flow around the square cylinder with stationary wall case; **(b)** *St* for the fluid flow around a square cylinder with stationary wall case; **(c)** C_d for the flow past a square cylinder with moving wall for Re = 100; **(d)** *St* for the flow past a square cylinder with moving wall for Re = 100.

G/A and S/A ratios are maintained while varying the aspect ratios (AR) to values of 1, 2, 3, 4, and 5, corresponding to a Reynolds number (*Re*) equal to 100.

Vorticity contours are displayed in Figures 5a–f for a complete cycle of the lift coefficient oscillation for a fixed inter-cylinder spacing to height ratio (S/A = 0.5) and a gap to height ratio (G/A = 0.5) for an aspect ratio (AR) of 1. It shows four different instants denoted as A, B, C and D, which correspond to various times within a vortex shedding cycle. These instants capture distinct moments during the cycle, where the period of the vortex shedding cycle is denoted as T. In the given flow scenario, the negative vorticity, representing clockwise rotation while the positive vorticity, indicating counter-clockwise rotation. The negative vortices originate from the top surface of the cylinder, while the positive ones emerge from the bottom of the cylinder. At an aspect ratio (AR) of 1, the shear layers that form along the wall combine with the positive shear layer created on the bottom surface of the cylinder. The merging of shear layers causes the vortices to elongate, resulting in a single, elongated vortex. Once the shedding of a single row of vortices occurs, shedding ceases, and the flow transitions into a quasi-steady state. The flow reaches a steady state while a steady wake is formed behind the cylinder. The elongation of the vortex observed is attributed to a shear-layer mixing process, whereby the upper and lower separated shear sheets interact and combine slowly with each other downstream. The moving wall enhances the strength of the lower shear layer to interact earlier with the upper layer, and the aspect ratio lowers the curvature and mutual induction of the two layers. Consequently, the two layers become more aligned with the streamwise direction and this form elongated vorticity structures rather than discrete vortex roll-up. This shear-layer behaviour, combined with shear-layer behaviour, undermines the establishment of coherent vortices and directly leads to the

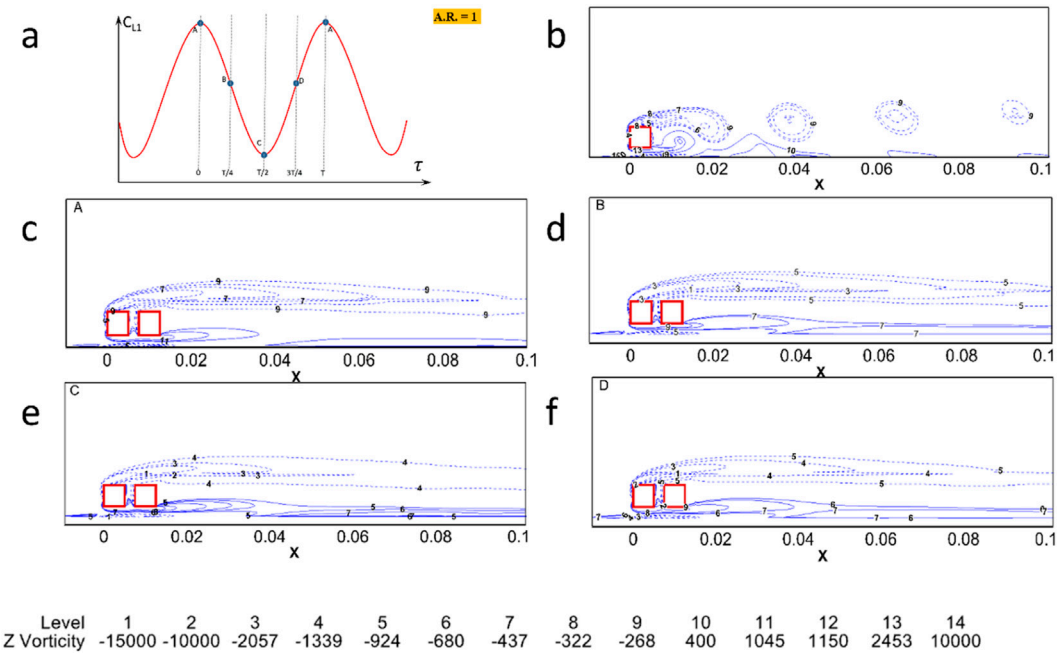

FIGURE 5
Vorticity contours plotted with AR = 1 for: **(a)** one cycle at different times (A, B, C, and D); **(b)** instantaneous time; **(c)** time instant A; **(d)** time instant B; **(e)** time instant C; and **(f)** Time instant D.

suppression of unsteadiness. In this quasi-steady state, the flow patterns remain relatively constant over time. A completely different pattern of vortex shedding can be observed in the case of an isolated cylinder for the same aspect ratio (AR = 1). A rolling pattern is observed in the vortex structure behind the cylinder, which separates from the main vortices and becomes weaker as it moves away from the cylinder. Aerodynamic forces, vortex shedding behavior, and wake generation are all significantly influenced by flow separation. Passive and active flow-control methods can have a substantial impact on separation features and reattachment locations, as noted in the recent review by Abdolahipour (2024).

Figures 6a–h show the vorticity contours plotted for single- and tandem-cylinder arrangements with aspect ratios ranging from 2 to 5. For an aspect ratio (AR) of 2, the length of the vortices is increased and swirling patterns become smoother with steady wake formation, as shown in Figures 6a–h. Rolling in the vortex pattern occurs behind the single cylinder, regardless of the aspect ratio, unlike in the tandem-cylinder case. With further increases in the AR (3, 4, and 5), negative vortices become steadier with increased length. Also, vortices originate from the bottom of the cylinder (positive vortices), continuously diminishing with increased aspect ratio, as in the single-cylinder case. A similar type of swirling pattern (vortices) is observed behind the tandem cylinders with increasing aspect ratios at fixed S/A and G/A ratios near a plane moving wall.

The current observations are applicable to the square cylinders where sharp corners hold the points of separation in place and enhance the formation of shear-layers. Circular cylinders by comparison have Reynolds-number-sensitive separation which results in more smooth wake transitions and may have a weaker moving-wall-induced stabilization. Depending on their aspect ratio, the rectangular cylinders are likely to exhibit earlier or later separation compared to the square counterpart and change the recirculation length and gap-flow characteristics. Thus, the basic principle of the wake-control phenomenon caused by the wall motion would be the same, however the strength of the drag reduction, lift suppression and shedding-frequency alteration would be different in the case of circular or rectangular geometries.

5.2 Time evolution of lift and drag coefficients

Figures 7, 8 depict changes in lift and drag coefficients over time. At low G/A and S/A ratios (0.5), and with an aspect ratio of 1, slight oscillations are observed in the C_L curve for both cylinders. Flow oscillations for the cylinder downstream are more pronounced compared to those observed for a single cylinder and the cylinder upstream, as depicted in Figures 7, 8. As the aspect ratio (AR) further increases (AR = 2, 3, 4, and 5), the oscillations in the C_L curves progressively decrease. With an increased aspect ratio, the lift coefficients for the upstream (C_{L1}) and downstream (C_{L2}) cylinders continuously increase. Figure 7f depicted the FFT spectrum analysis of the lift coefficient of the single cylinder at $AR = 1$ and $AR = 2$, indicating that the dominant peak is sharp. To ensure statistically converged force coefficients, the mean and RMS values of C_L and C_d are calculated once the relative change between subsequent time-averaging is less than 1%.

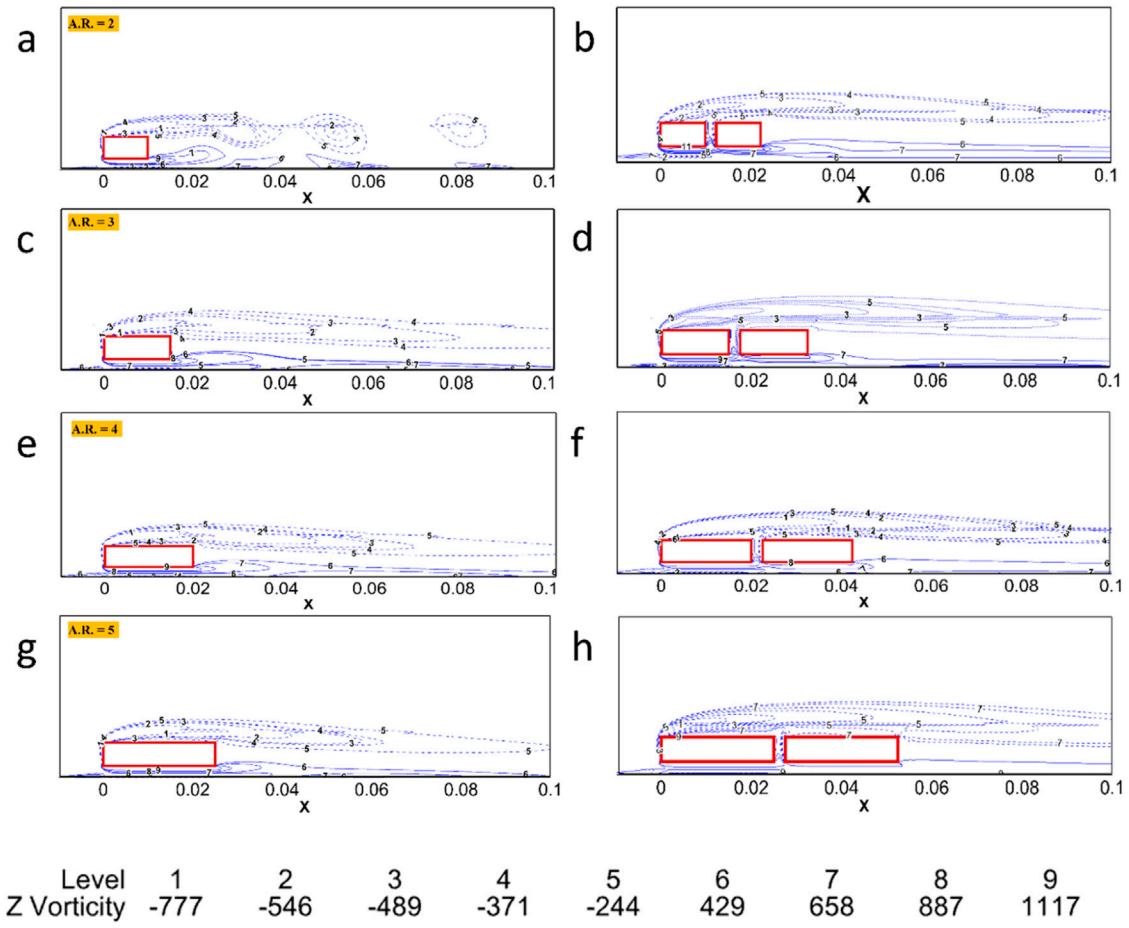

FIGURE 6
Instantaneous vorticity contours plotted for: **(a,b)** aspect ratio = 2; **(c,d)** aspect ratio = 3; **(e,f)** aspect ratio = 4; and **(g,h)** aspect ratio = 5.

Figure 8 illustrates the time progression of the drag coefficient at constant G/A and S/A ratios, both equal to 0.5. The graph shows how the drag coefficient changes as the aspect ratio varies between 1 and 5. At an aspect ratio of 1, there are slight oscillations observed in the C_{d1} and C_{d2} curves, but these oscillations are significantly smaller compared to the case of a single cylinder. As the aspect ratio increases to 2, the oscillations vanish, while small oscillations can be observed in the isolated cylinder case. When the aspect ratio is further increased to 3, 4, and 5, the oscillations in the lift coefficient curves completely disappear, and similar patterns can be observed in the case of a single cylinder.

5.3 Strouhal number (*St*)

The Strouhal number (*St*), denoted as fA/U_∞, provides more insight into the existence or suppression of vortex shedding. It serves as a measure of the frequency of vortex shedding in an oscillating flow. The vortex shedding frequency, denoted as f, can be determined by calculating the reciprocal of the time interval between two consecutive cycles of vortex shedding. This interval is typically measured based on the oscillations in the lift coefficient. In this study, no oscillations are observed in the curves of the lift coefficients (C_{L1} and C_{L2}) except at an aspect ratio of 1. This indicates steady wake formation behind the cylinders.

5.4 Instantaneous streamline contours

Figure 9 illustrates instantaneous streamline contours focusing on the flow across tandem cylinders located closer to the moving wall. At an aspect ratio of 1, the flow exhibits a significant recirculation in the wake area, originating from the upper corner of the front face of the upstream cylinder. The stability of this elongated recirculation is disrupted, resulting in noticeable unsteadiness characterized by weak oscillations in the flow behind the cylinders. This observation suggests that at an aspect ratio of 1, tandem cylinders tend to behave as a single cylinder, as indicated by their collective flow characteristics.

As the aspect ratio further increases (AR = 2, 3, 4, and 5), the flow remains steady without exhibiting significant oscillations. A slight change in the vortex structure can be observed in the case of a single cylinder with an aspect ratio of 2, exhibiting a rolling pattern in the vortices that stretches with the flow. The flow field continues

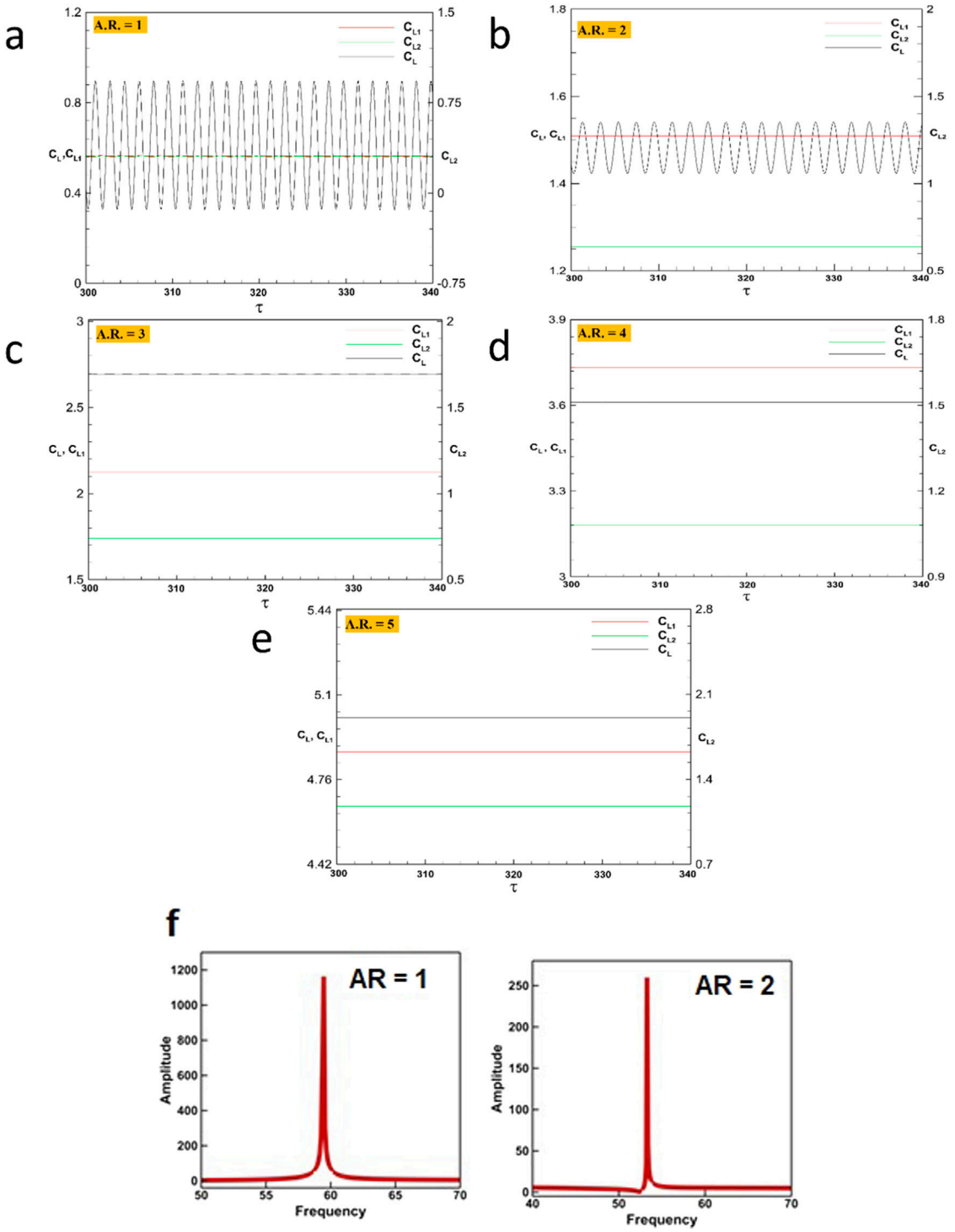

FIGURE 7
The time evolution of the lift coefficients of the single cylinder (C_L), and for tandem cylinders, upstream (C_{L1}) and downstream (C_{L2}) cylinders with fixed S/A and G/A ratios is shown at an: **(a)** aspect ratio = 1; **(b)** aspect ratio = 2; **(c)** aspect ratio = 3; **(d)** aspect ratio = 4; and **(e)** aspect ratio = 5, **(f)** FFT analysis of C_L for single cylinder with AR 1 and 2.

to be characterized by the presence of a persistent wake region, which remains unchanged, along with two asymmetric recirculation zones behind each cylinder. At aspect ratios of 4 and 5, an increase in the length of the wake behind the downstream cylinder is observed, while the wake region between the cylinders decreases in size, similar to the single-cylinder case.

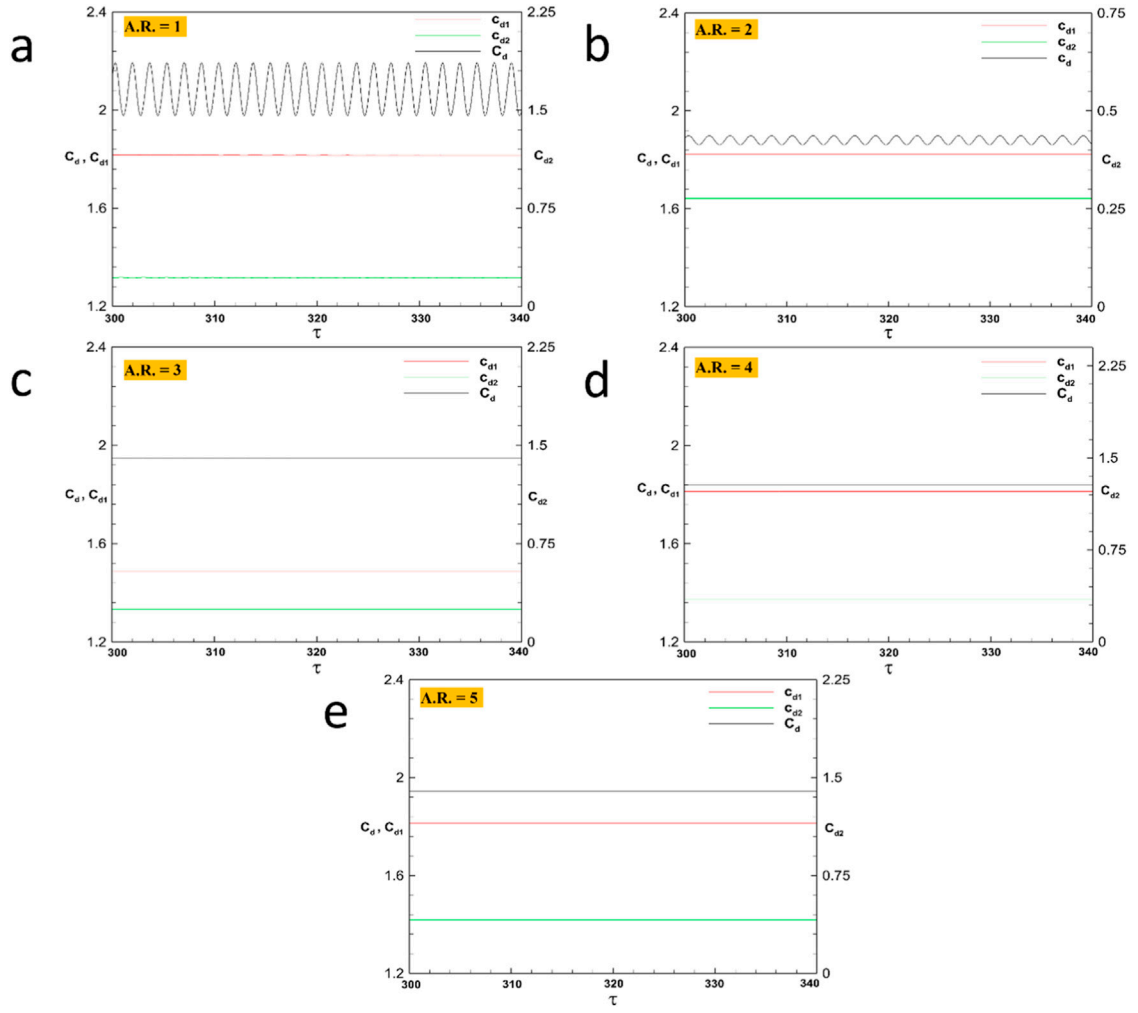

FIGURE 8
The time evolution of the drag coefficients of the single cylinder (C_d) and for tandem cylinders, upstream (C_{d1}) and downstream (C_{d2}) cylinders with fixed S/A and G/A ratios is shown at an: **(a)** aspect ratio = 1; **(b)** aspect ratio = 2; **(c)** aspect ratio = 3; **(d)** aspect ratio = 4; and **(e)** aspect ratio = 5.

5.5 Time-averaged lift and drag coefficients

Figure 10 illustrates the changes in the average values of lift (C_L) and drag (C_d) over time. Lift and drag coefficients for the upstream and downstream cylinders are shown by the solid red and green lines, respectively. The single cylinder is indicated by a solid blue line. The figure demonstrates that the lift and drag forces acting on the upstream cylinder are similar to those on a single cylinder. The downstream cylinder experiences lower forces compared to the upstream cylinder. With an increased aspect ratio from 1 to 5, the lift coefficient for the upstream cylinder (C_{L1}) and single cylinder (C_L) increased considerably, but for the downstream cylinder (C_{L2}), the increase was slight. Similar values of the drag coefficient can be observed for the upstream cylinder (C_{d1}) and single cylinder (C_d) with increased aspect ratios. However, the drag coefficient for a downstream cylinder (C_{d1}) is much lower than either C_{d2} or C_d.

Our observations indicate that the lift and drag coefficients are highest for the upstream cylinder, followed by a single cylinder, and lowest for the downstream cylinder. When a square cylinder is positioned behind another square cylinder, both moving at the same speed, specific values can ensure reduced drag force and a stable flow across the downstream cylinder. This principle is frequently employed in intelligent fuel transport systems. All aspect ratios show the downstream cylinder to have lower mean drag than the upstream cylinder. Such action is mainly because of the sheltering effect of the upstream cylinder that causes the downstream body to be in its wake and recirculation zone. Consequently, a lower effective inflow velocity and reduced pressure gradients are exposed to the downstream cylinder, and pressure drag is reduced. This wake shielding continues through all experimented aspect ratios keeping the drag to the downstream cylinder much lower.

The impact of the moving wall on the flow physics can be explained by its effect on the near-wall mean shear, which controls the energy transfer between the mean flow and fluctuations. The moving wall enhances the lower shear layer and, thereby, diminishes the generation of oscillating kinetic energy, as well as roll-up of coherent vortices. This process aids in reducing unsteadiness with aspect ratio, and in the current setup ($Re = 100$, $S/A = G/A = 0.5$), the

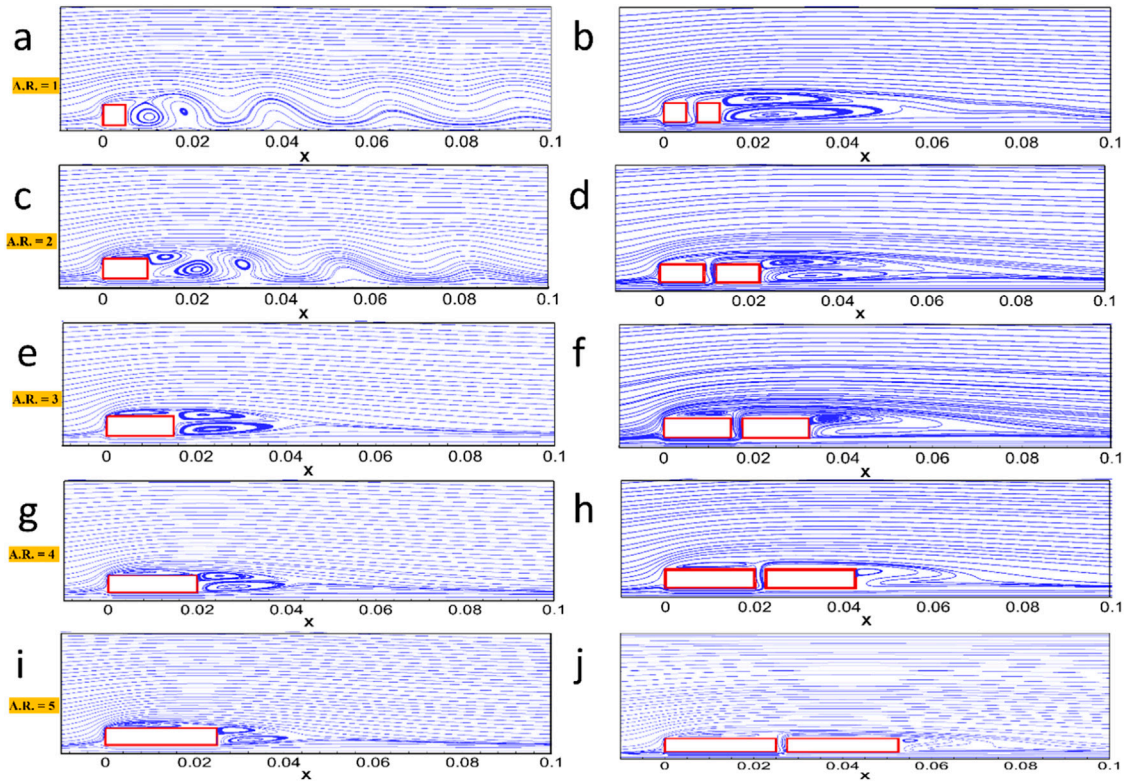

FIGURE 9
Instantaneous streamlines in the wake of single and tandem cylinders for fixed S/A and G/A values of 0.5 for different aspect ratios at a particular time: **(a,b)** aspect ratio = 1; **(c,d)** aspect ratio = 2; **(e,f)** aspect ratio = 3; **(g,h)** aspect ratio = 4; and **(i,j)** aspect ratio = 5.

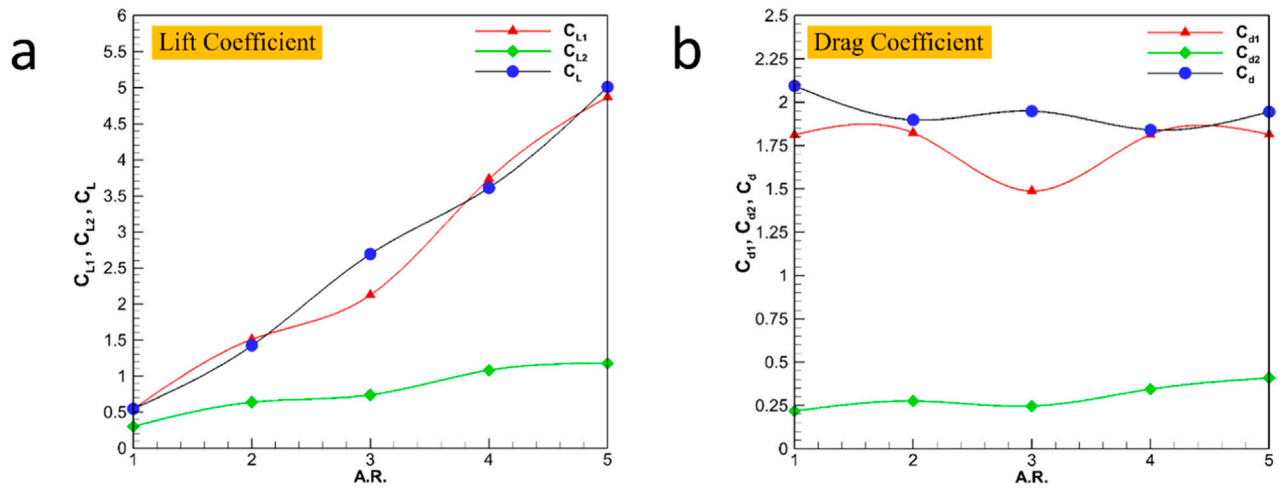

FIGURE 10
(a) Lift coefficient of single cylinder (C_L) and for tandem cylinders, upstream (C_{L1}) and downstream (C_{L2}), as a function of aspect ratio (AR) at fixed G/A and S/A ratios (0.5); **(b)** drag coefficient of single cylinder (C_d) and for tandem cylinders, upstream (C_{d1}) and downstream (C_{d2}), as a function of aspect ratio (AR) at fixed G/A and S/A ratios (0.5).

wake has become effectively steady at $AR = 3$. This value represents an effective suppression level under the study conditions, but a formal definition of absolute instability would require a biglobal or global stability analysis, which is beyond the scope of this work.

The strength of the vortex shedding, which provides evidence of suppression, was measured by assessing the strength of the vortex circulation (Γ) for each configuration by integrating the absolute vorticity over the near-wake of the cylinders. As Figure 11

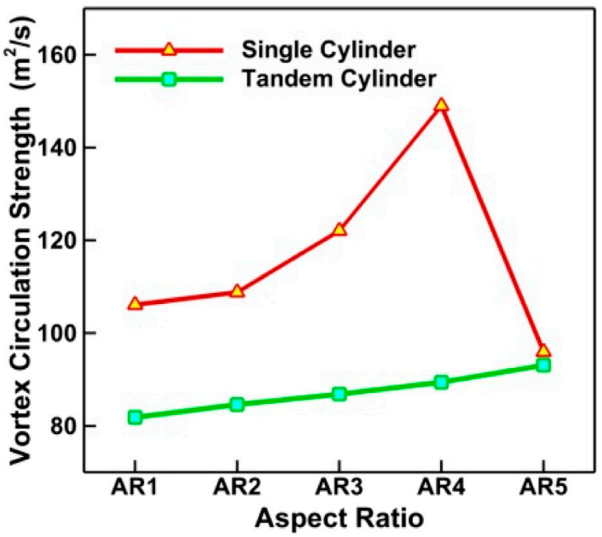

FIGURE 11
Recirculation vortex strength for single and tandem cylinders at all AR.

demonstrates, there is an uninterrupted rise in Γ between $AR = 1$ and $AR = 4$ in the single-cylinder case, at which point there is a sharp drop in Γ, since the wake has reorganized. However, the opposite can be seen in the tandem-cylinder arrangement, where the circulation level is always relatively lower, and Γ grows between $AR = 1$ and $AR = 5$ only slowly, being much less than that of the isolated cylinder. The decreased magnitude of circulation directly represents less vigorous shear-layer roll-up and Coherence of the vortex. The high contrast between the two cases quantitatively demonstrates that with the introduction of the moving wall, the initial shear-layer mixing inhibits the rotational energy of the wake, preventing the development of periodic vortex shedding. These findings support the previous qualitative observations of the vorticity and streamline fields, providing a quantifiable measure of the suppression mechanism.

6 Comparison with the previous stationary wall study

To highlight the influence of wall motion, the existing results were compared with the tandem set up of Chatterjee and Mondal (2012) at $Re = 100$ with their tabulated results of drag and Strouhal data at the closest spacing ratio, that is, S/A = 0.5 in the current study. Table 4 gives the most important quantities in a table. In the moving-wall example, the mean drag (C_{d1}) at the upstream cylinder is larger ($C_{d1} = 1.83$) than in the stationary, unconfined tandem configuration of Chatterjee and Mondal (2012) ($C_{d1} = 1.6$ at similar *Re* and spacing) that is due to greater shear near the wall and greater momentum exchange against it due to the wall motion. On the contrary, the downstream cylinder in the current experiment experiences a significantly lower drag ($C_{d2} = 0.21$) as well as virtually no oscillations of the lift rather than the expected significantly greater downstream drag and nearly inaudible periodic fluctuations in the lift once the spacing is beyond their critical value, indicative of continued wake unsteadiness in the stationary-wall case.

7 Conclusion

Numerical simulations were conducted to investigate the flow characteristics around tandem cylinders placed very close to a moving wall. The plane wall is moving with the same velocity as the fluid entering from the inlet. This study considered various aspect ratios ranging from 1 to 5, while maintaining a fixed cylinder-to-wall gap ratio (G/A = 0.5) and inter-cylinder spacing ratio (S/A = 0.5). The Reynolds number (*Re*) of 100 was used in the entire study. The presence of a moving wall has a significant influence on the flow dynamics around and between the tandem cylinders. The finite volume method was used for performing numerical simulations based on the SIMPLE algorithm. The study yielded several significant conclusions, which are summarized as follows:

1. For an aspect ratio of 1, merging of shear layers takes place, which originates from the top and bottom sides of the cylinder, causing the vortices to elongate. This results in a single row of vortices, generating a pattern that remains constant over time. With increased aspect ratios (2, 3, 4, and 5), the length of vortices increased and became smoother with steady wake formation. Additionally, positive vortices that originate from the bottom of the cylinder continuously decrease in magnitude with increasing aspect ratios.
2. In the context of streamline contours, a significant recirculation in the wake area is observed for an aspect ratio of 1. Tandem cylinders tend to behave as an isolated cylinder. With increased aspect ratios, flow remains steady without exhibiting significant oscillations.

TABLE 4 C_D, C_L and *St* values comparison with the stationary wall study.

Parameter	Present study (Moving wall)	Stationary wall (Chatterjee and Mondal, 2012)
C_{d1} (Upstream)	1.83	1.6
C_{d2} (Downstream)	0.21	0.95
C_{L1} (Upstream)	Very small oscillation	Higher oscillation amplitude
C_{L2} (Downstream)	Nearly zero/Suppressed	Moderate oscillation
St	0.110	Steady flow

3. The drag (C_d) and lift (C_L) coefficients exhibit a chaotic pattern for the upstream cylinder, whereas the downstream cylinder displays a consistent trend, unlike the single cylinder case. This happens due to the very close proximity of the cylinders to the moving wall and a much smaller gap between the cylinders. The single cylinder has the highest drag coefficient (C_d), unlike the lift coefficient (C_L). Also, the upstream cylinder exhibits a higher drag coefficient (C_{d1}) than the downstream cylinder (C_{d2}), which has the lowest drag coefficient among all cylinders examined.
4. The measured decreases in drag and lift oscillations are attributed to the interaction of shear layers because of the moving wall and the cylinders. By stabilizing the wake and stretching vortices, this shear coupling stops vortex shedding. The switch to steady wake conditions is associated with the critical ratios of cylinder spacing and wall gap observed in past literature and verifies our results. The phenomenon of vortex suppression is mostly due to the interaction of shear layers by the motion of the wall, as opposed to viscous damping. Although the 2D laminar model cannot capture three-dimensional and turbulent wake complexities, the shear alignment core mechanism of wake control is likely to remain in the more realistic flows. Future research should extend this work to three-dimensional (3D) turbulent simulations to comprehensively investigate these effects.

8 Recommendations for future research

The future research will focus on broadening the current numerical model with the help of the recent progress in flow-physics observations found in the literature (Majeed et al., 2024; Refaie Ali et al., 2024a; Saleem et al., 2024; Ali et al., 2024; Refaie Ali et al., 2024b; Refaie Ali et al., 2025; Ghayoor et al., 2024; Refaie Ali et al., 2024c). These papers note the advancements in the bluff-body aerodynamics, moving-boundary effects, and the strategy of managing the wake-flow, which can complement and add to the current findings. When combined with these methods in simulations in the future, it will be possible to compare a wider range of geometries, boundary conditions and flow regimes which will enhance the applicability and generality of the results produced. The modeling of the current flow-behavior knowledge into an applicable control method, such as active suction/blowing in the immediate vicinity of the separation regions and surface treatments that can recreate the momentum-enhancing influence of wall movement will be addressed in future work. The methods can provide useful drag-reduction and wake-stabilization methods to engineering systems.

Future studies should expand the investigation to three-dimensional simulations to account for the dynamics of transverse vortices and spanwise instabilities, which the existing 2D model does not reproduce. The dynamic coupling of wall motion and the flow field, as well as complete fluid-structure interaction modelling, would provide insight into feedback mechanisms between bluff body wakes and boundary deformation, as applied to applications such as flexible underbodies in vehicles or compliant marine structures. Further research can be conducted on higher Reynolds numbers, varying wall velocities, and the experimental validation of this research using PIV, which will include the comparison between numerical and real-world tandem bluff body flows around moving surfaces. To design predictive models of flow control and heat transfer performance in complex geometries, future studies can combine data-driven methods, including Artificial Intelligence and machine learning approaches. The effectiveness of similar thermal fluid systems with such methods has been proven in recent studies and gives a promising direction to expand the current work (Shafiq et al., 2025; Shafiq et al., 2022).

Data availability statement

The raw data supporting the conclusions of this article will be made available by the authors, without undue reservation.

Author contributions

PK: Formal Analysis, Investigation, Conceptualization, Data curation, Validation, Visualization, Writing – original draft. SC: Conceptualization, Formal Analysis, Investigation, Visualization, Methodology, Supervision, Writing – review and editing. NP: Data curation, Investigation, Writing – original draft. HJ: Methodology, Software, Writing – original draft. SR: Validation, Visualization, Writing – original draft. MK: Investigation, Writing – review and editing, Software, Validation. VC: Investigation, Writing – review and editing, Formal Analysis, Funding acquisition, Resources. SE: Formal Analysis, Supervision, Writing – review and editing.

Funding

The author(s) declared that financial support was received for this work and/or its publication. The research on "Analysis of fluid flow across a 2D bluff body in a tandem arrangement with varying aspect ratios near a moving wall" by King Mongkut's Institute of Technology Ladkrabang (KMITL) received funding support from the NSRF (FRB660065/0258-RE-KRIS/RE-KRIS/FF66/43).

Conflict of interest

The author(s) declared that this work was conducted in the absence of any commercial or financial relationships that could be construed as a potential conflict of interest.

Generative AI statement

The author(s) declared that generative AI was not used in the creation of this manuscript.

Any alternative text (alt text) provided alongside figures in this article has been generated by Frontiers with the support of artificial intelligence and reasonable efforts have been made to ensure accuracy, including review by the authors wherever possible. If you identify any issues, please contact us.

Publisher's note

References

Abbasi, W. S., Ehsan, M., Rahman, H., Uddin, Z., Hassan, M. M., and Saleem, K. (2024). Analysis of the wake mechanism in external flow around tandem bluff bodies with different aspect ratios. *Front. Mech. Eng.* 10, 1341618. doi:10.3389/fmech.2024.1341618

Abdolahipour, S. (2023). Effects of low and high frequency actuation on aerodynamic performance of a supercritical airfoil. *Front. Mech. Eng.* 9, 1290074. doi:10.3389/fmech.2023.1290074

Abdolahipour, S. (2024). Review on flow separation control: effects of excitation frequency and momentum coefficient. *Front. Mech. Eng.* 10, 1380675. doi:10.3389/fmech.2024.1380675

Abdolahipour, S., Mani, M., and Shams Taleghani, A. (2022a). Pressure improvement on a supercritical high-lift wing using simple and modulated pulse jet vortex generator. *Flow Turbul. Combust.* 109, 65–100. doi:10.1007/s10494-022-00327-9

Abdolahipour, S., Mani, M., and Shams Taleghani, A. (2022b). Experimental investigation of flow control on a high-lift wing using modulated pulse jet vortex generator. *J. Aerosp. Eng.* 35, 05022001. doi:10.1061/(asce)as.1943-5525.0001463

Ahmed, S. R., Ramm, G., and Faltin, G. (1984). Some salient features of the time-averaged ground vehicle wake. *SAE Transactions*, 473–503. Available online at: https://www.jstor.org/stable/44434262.

Akansu, Y. E., and Fırat, E. (2010). Control of flow around a square prism by slot jet injection from the rear surface. *Exp. Therm. Fluid Sci.* 34, 906–914. doi:10.1016/j.expthermflusci.2010.02.007

Ali, A. R., Rafique, K., Imtiaz, M., Jan, R., Alotaibi, H., and Mekawy, I. (2024). Exploring magnetic and thermal effects on MHD bio-viscosity flow at the lower stagnation point of a solid sphere using keller box technique. *Partial Differ. Equations Appl. Math.* 9, 100601. doi:10.1016/j.padiff.2023.100601

Anthony, F. M., and Turnock, S. R. (2007). Marine rudders and control surfaces.

Barry, N., Burton, D., Sheridan, J., Thompson, M., and Brown, N. A. (2016). Flow field interactions between two tandem cyclists. *Exp. Fluids* 57, 1–14. doi:10.1007/s00348-016-2273-y

Bearman, P. W. (1984). Vortex shedding from oscillating bluff bodies. *Annu. Review Fluid Mechanics* 16, 195–222. doi:10.1146/annurev.fluid.16.1.195

Bearman, P., and Zdravkovich, M. (1978). Flow around a circular cylinder near a plane boundary. *J. Fluid Mech.* 89, 33–47. doi:10.1017/s002211207800244x

Bhattacharyya, S., and Maiti, D. (2005). Vortex shedding from a square cylinder in presence of a moving wall. *Int. Journal Numerical Methods Fluids* 48, 985–1000. doi:10.1002/fld.970

Chatterjee, D., and Mondal, B. (2012). Forced convection heat transfer from tandem square cylinders for various spacing ratios. *Numer. Heat. Transf. Part A Appl.* 61, 381–400. doi:10.1080/10407782.2012.647985

Chen, W., Ji, C., Xu, D., and Zhang, Z. (2020). Vortex-induced vibrations of two inline circular cylinders in proximity to a stationary wall. *J. Fluids Struct.* 94, 102958. doi:10.1016/j.jfluidstructs.2020.102958

Cheng, M., Tan, S., and Hung, K. (2005). Linear shear flow over a square cylinder at low reynolds number. *Phys. Fluids* 17, 078103. doi:10.1063/1.1953727

Cheng, M., Whyte, D., and Lou, J. (2007). Numerical simulation of flow around a square cylinder in uniform-shear flow. *J. Fluids Structures* 23, 207–226. doi:10.1016/j.jfluidstructs.2006.08.011

Davis, R., and Moore, E. (1982). A numerical study of vortex shedding from rectangles. *J. Fluid Mech.* 116, 475–506. doi:10.1017/s0022112082000561

Dhinakaran, S. (2011). Heat transport from a bluff body near a moving wall at Re= 100. *Int. Journal Heat Mass Transfer* 54, 5444–5458. doi:10.1016/j.ijheatmasstransfer.2011.07.046

Franke, R., Rodi, W., and Schönung, B. (1990). Numerical calculation of laminar vortex-shedding flow past cylinders. *J. Wind Eng. Industrial Aerodynamics* 35, 237–257. doi:10.1016/0167-6105(90)90219-3

Ghayoor, M., Abbasi, W. S., Majeed, A. H., Alotaibi, H., and Ali, A. R. (2024). Interference effects on wakes of a cluster of pentad square cylinders in a crossflow: a lattice boltzmann study. *AIP Adv.* 14, 125111. doi:10.1063/5.0239176

Huang, W.-X., and Sung, H. J. (2007). Vortex shedding from a circular cylinder near a moving wall. *J. Fluids Struct.* 23, 1064–1076. doi:10.1016/j.jfluidstructs.2007.02.004

Hucho, W.-H. (2013). *Aerodynamics of road vehicles: from fluid mechanics to vehicle engineering*. Elsevier.

Hwang, R. R., and Sue, Y. (1998). "Numerical simulation for shear effect on vortex shedding behind a square cylinder," in *Proceedings of the ISOPE international ocean and polar engineering conference*.

Kalita, J. C., and Ray, R. K. (2009). A transformation-free HOC scheme for incompressible viscous flows past an impulsively started circular cylinder. *J. Computational Physics* 228, 5207–5236. doi:10.1016/j.jcp.2009.04.016

Kiya, M., Tamura, H., and Arie, M. (1980). Vortex shedding from a circular cylinder in moderate-reynolds-number shear flow. *J. Fluid Mech.* 101, 721–735. doi:10.1017/s0022112080001899

Lankadasu, A., and Vengadesan, S. (2008). Onset of vortex shedding in planar shear flow past a square cylinder. *Int. J. Heat Fluid Flow* 29, 1054–1059. doi:10.1016/j.ijheatfluidflow.2008.02.016

Lankadasu, A., and Vengadesan, S. (2011). Shear effect on square cylinder wake transition characteristics. *Int. Journal Numerical Methods Fluids* 67, 1115–1134. doi:10.1002/fld.2408

Majeed, A. H., Liu, D., Ali, A. R., Alotaibi, H., Yin, Z. J., and Yi, R. H. (2024). Numerical simulations of energy storage performance in a close configuration: a galerkin finite element-based computation. *Alex. Eng. J.* 104, 56–65. doi:10.1016/j.aej.2024.06.037

Norberg, C. (1993). Flow around rectangular cylinders: pressure forces and wake frequencies. *J. Wind Engineering Industrial Aerodynamics* 49, 187–196. doi:10.1016/0167-6105(93)90014-f

Okajima, A. (1982). Strouhal numbers of rectangular cylinders. *J. Fluid Mechanics* 123, 379–398. doi:10.1017/s0022112082003115

Raghunathan, R. S., Kim, H.-D., and Setoguchi, T. (2002). Aerodynamics of high-speed railway train. *Prog. Aerosp. Sciences* 38, 469–514. doi:10.1016/s0376-0421(02)00029-5

Rahman, M. M., Karim, M. M., and Alim, M. A. (2007). Numerical investigation of unsteady flow past a circular cylinder using 2-D finite volume method. *J. Nav. Archit. Mar. Eng.* 4, 27–42. doi:10.3329/jname.v4i1.914

Rajpoot, R. S., Anirudh, K., and Dhinakaran, S. (2021). Numerical investigation of unsteady flow across tandem square cylinders near a moving wall at re= 100. *Case Stud. Therm. Eng.* 26, 101042. doi:10.1016/j.csite.2021.101042

Refaie Ali, A., Abbasi, W. S., Younus, R., Rahman, H., Nadeem, S., Majeed, A. H., et al. (2024a). Enhancing hydrodynamic forces through miniaturized control of square cylinders using the lattice boltzmann method. *Sci. Rep.* 14, 15524. doi:10.1038/s41598-024-65423-4

Refaie Ali, A., Mahmood, R., Asghar, A., Majeed, A. H., and Behiry, M. H. (2024b). AI-based predictive approach *via* FFB propagation in a driven-cavity of ostwald de-Waele fluid using CFD-ANN and levenberg–marquardt. *Sci. Rep.* 14, 11024. doi:10.1038/s41598-024-60401-2

Refaie Ali, A., Mahmood, R., Ishfaq, M., Rehman, N., and Majeed, A. H. (2024c). Optimization of heat transfer in a double lid-driven cavity with isoperimetric heated blocks using GFEM. *Sci. Rep.* 14, 28168. doi:10.1038/s41598-024-78525-w

Refaie Ali, A., Siddig, N. H., Irshad, S., Abu-Nab, A. K., and Majeed, A. H. (2025). Investigating magnetized double-diffusive flow: heat-mass transfer dynamics and thermal radiation based on the shooting method. *J. Nonlinear Math. Phys.* 32, 37. doi:10.1007/s44198-025-00283-8

Robichaux, J., Balachandar, S., and Vanka, S. P. (1999). Three-dimensional floquet instability of the wake of square cylinder. *Phys. Fluids* 11, 560–578. doi:10.1063/1.869930

Saha, A. K. (2013). Unsteady flow past a finite square cylinder mounted on a wall at low reynolds number. *Comput. and Fluids* 88, 599–615. doi:10.1016/j.compfluid.2013.10.010

Saha, A. K., and Shrivastava, A. (2015). Suppression of vortex shedding around a square cylinder using blowing. *Sadhana* 40, 769–785. doi:10.1007/s12046-014-0331-9

Saleem, M., Majeed, A. H., Ahmad, I., and Refaie Ali, A. (2024). Symmetry-based analysis of nonlinear mixed convection in 3D EMHD nano-carreau fluid flow with Riga stretched surface effects and multi-physical interactions. *ZAMM-Journal Appl. Math. Mechanics/Zeitschrift für Angewandte Math. und Mech.* 104, e202400072. doi:10.1002/zamm.202400072

Sarkar, S., Mondal, C., Manna, N. K., and Saha, S. K. (2021). Forced convection past a semi-circular cylinder at incidence with a downstream circular cylinder: thermofluidic transport and stability analysis. *Phys. Fluids* 33, 023603. doi:10.1063/5.0039167

Sasmal, C., and Chhabra, R. (2011). Laminar natural convection from a heated square cylinder immersed in power-law liquids. *J. Newt. Fluid Mech.* 166, 811–830. doi:10.1016/j.jnnfm.2011.04.013

Schlichting, H., and Gersten, K. (2017). Boundary-layer theory.

Sen, S., Mittal, S., and Biswas, G. (2011). Flow past a square cylinder at low reynolds numbers. *Int. J. Numer. Methods Fluids* 67, 1160–1174. doi:10.1002/fld.2416

Seo, J., Yun, J., and Lee, J. (2023). Control of turbulent flow over a circular cylinder using tabs. *Mathematics* 11, 968. doi:10.3390/math11040968

Shams Taleghani, A., and Izadi, M. (2025). Multiobjective optimization of a single slotted flap using artificial neural network and metaheuristic algorithms. *J. Eng. Mech.* 151, 05025001. doi:10.1061/jenmdt.emeng-8015

Shafiq, A., Çolak, A. B., and Sindhu, T. N. (2022). Optimization of bioconvective magnetized Walter's b nanofluid flow towards a cylindrical disk with artificial neural networks. *Lubricants* 10, 209. doi:10.3390/lubricants10090209

Shafiq, A., Çolak, A. B., Sindhu, T. N., and Abushal, T. A. (2025). Investigating the sensitivity of nanofluid flow around a cylindrical disk: a study of Walter's B nanofluid using response surface methodology and artificial neural networks. *J. Eng. Res.* 13, 3781–3793. doi:10.1016/j.jer.2024.12.010

Shams Taleghani, A., and Torabi, F. (2025). Recent developments in aerodynamics. *Front. Mech. Eng.* 10, 1537383. doi:10.3389/fmech.2024.1537383

Sharma, A., and Eswaran, V. (2004). Heat and fluid flow across a square cylinder in the two-dimensional laminar flow regime. *Numer. Heat. Transf. Part A Appl.* 45, 247–269. doi:10.1080/10407780490278562

Shimizu, Y., and Tanida, Y. (1978). Fluid forces acting on cylinders of rectangular cross-section. *Trans. JSME B* 44, 2699–2706. doi:10.1299/kikai1938.44.2699

Sohankar, A. (2008). Large eddy simulation of flow past rectangular-section cylinders: side ratio effects. *J. Wind Engineering Industrial Aerodynamics* 96, 640–655. doi:10.1016/j.jweia.2008.02.009

Sohankar, A., Norberg, C., and Davidson, L. (1998). Low-Reynolds-number flow around a square cylinder at incidence: study of blockage, onset of vortex shedding and outlet boundary condition. *Int. Journal Numerical Methods Fluids* 26, 39–56. doi:10.1002/(sici)1097-0363(19980115)26:1<39::aid-fld623>3.0.co;2-p

Squires, T. M., and Quake, S. R. (2005). Microfluidics: fluid physics at the nanoliter scale. *Rev. Modern Physics* 77, 977–1026. doi:10.1103/revmodphys.77.977

Taleghani, A. S., Hesabi, A., and Esfahanian, V. (2025). Numerical study of flow control to increase vertical tail effectiveness of an aircraft by tangential blowing. *Int. J. Aeronautical Space Sci.* 26, 785–799. doi:10.1007/s42405-024-00826-1

Wu, Z., and Choi, H. (2021). Modification of flow behind a circular cylinder by steady and time-periodic blowing. *Phys. Fluids* 33, 115126. doi:10.1063/5.0067706

Yang, W., and Stremler, M. A. (2019). Critical spacing of stationary tandem circular cylinders at re≈ 100. *J. Fluids Struct.* 89, 49–60. doi:10.1016/j.jfluidstructs.2019.02.023

Yen, S.-C., San, K., and Chuang, T. (2008). Interactions of tandem square cylinders at low reynolds numbers. *Exp. Therm. Fluid Sci.* 32, 927–938. doi:10.1016/j.expthermflusci.2007.07.001

Zhang, L., and Balachandar, S. (2006). Onset of vortex shedding in a periodic array of circular cylinders. *J. Fluids Eng.* 128, 1101–1105. doi:10.1115/1.2201630

Zhang, X.-F., Yang, J.-C., Ni, M.-J., Zhang, N.-M., and Yu, X.-G. (2022). Experimental and numerical studies on the three-dimensional flow around single and two tandem circular cylinders in a duct. *Phys. Fluids* 34, 033610. doi:10.1063/5.0084764

Zhao, M. (2021). Flow past a circular cylinder and a downstream sphere for re< 300. *J. Fluid Mech.* 913, A20. doi:10.1017/jfm.2020.1123

Zhu, H., Zhao, H., and Zhou, T. (2019). Direct numerical simulation of flow over a slotted cylinder at low reynolds number. *Appl. Ocean Res.* 87, 9–25. doi:10.1016/j.apor.2019.01.019

Zhu, H., Chen, Q., Tang, T., Alam, M. M., and Zhou, T. (2023). Flow structures around a circular cylinder with bilateral splitter plates and their dynamic characteristics. *Ocean. Eng.* 269, 113547. doi:10.1016/j.oceaneng.2022.113547

Žkauskas, A. (1987). Heat transfer from tubes in crossflow. *Adv. Heat Transfer* 18, 87–159. doi:10.1016/s0065-2717(08)70118-7

Nomenclature

A	Height of the cylinder (m)
B	Width of the cylinder (m)
C_d	Drag coefficient
C_L	Lift coefficient
f	Frequency of vortex shedding (Hz)
F_D	Drag force per unit length of cylinder (N m^{-1})
F_L	Lift force per unit length of cylinder (N m^{-1})
FFT	Fast Fourier Transform
G	Vertical gap between the cylinder and the moving wall, [m]
G/A	Gap ratio
Re	Reynolds number = U∞·A/ν
RMS	Root mean square
S	Streamwise spacing between cylinder centers (m)
S/A	Spacing ratio
St	Strouhal number = f·A/U∞
t	Time (s)
U_∞	Free stream velocity (m/s)
VIV	Vortex-induced vibration

Greek symbols

ν	Kinematic viscosity (m^2/s)
ρ	Fluid density (kg/m^3)
Δ	Difference (used in peak-to-peak)